ISSN 2228-9860 eISSN 1906-9642 CODEN: ITJEA8

International Transaction Journal of Engineering, Management, & Applied Sciences & Technologies

http://TuEngr.com

Detection and Discrimination Modeling of Cells in Droplet Using Impedance Spectroscopy-Based Microfluidic System

Shabbir Chowdhury[1], Mohammad Asif Hussain[1], Nebras Sobahi[1*]

[1] Department of Electrical and Computer Engineering, King Abdulaziz University, Jeddah, 21589, SAUDI ARABIA.
**Corresponding author (Email: nsobahi@kau.edu.sa).*

Paper ID: 13A3Q

Volume 13 Issue 3

Received 21 November 2021
Received in revised form 01 March 2022
Accepted 08 March 2022
Available online 15 March 2022

Keywords:
Microfluidics; Microdroplets; Impedance-spectroscopy; Droplet; Cell counting; Cell in the droplet; Cell detection; Microfluidic chip.

Abstract

Cells in the droplet can be detected and characterized using an impedance spectroscopy-based microfluidic characterization technique that is relatively low-cost and efficient and brings several benefits to biomedical and biological research. In this modeling analysis, the two types of cells were differentiated and counted using a microfluidic impedance spectroscopy-based system. For this purpose, the optimal frequency and condition were characterized and determined. The impedance difference between wild-type and mutant yeast cells was found as 20.91Ω for the spherical-shaped droplet. For larger microdroplets, the squeezed shape droplets were considered, and in which condition, the difference became 14.42Ω which makes this model practically implementable for a large number of cells in droplet studies. This model can easily count the cells in the droplets based on the electrical impedance. This cost-effective design can dramatically improve cell sorting, counting, and separation. Further, the sensitivity can be amplified after the detection period to a reasonable state if needed.

Disciplinary: Biomedical Engineering, Cell Technology (Cell Biology, Cell Therapy).

Cite This Article:

Chowdhury, S., Hussain, M. A., and Sobahi, N. (2022). Detection and Discrimination Modeling of Cells in Droplet Using Impedance Spectroscopy-Based Microfluidic System. *International Transaction Journal of Engineering, Management, & Applied Sciences & Technologies, 13*(3), 13A3Q, 1-15. http://TUENGR.COM/V13/13A3Q.pdf DOI: 10.14456/ITJEMAST.2022.59

1 Introduction

Dielectric impedance spectroscopy has successfully been applied in Microfluidics systems to characterize any kind of material such as solid, liquid, and gaseous [1–3]. The dielectric properties of materials change depending on the type of material and frequency used for analysis. As it is

known, the electric field from the stimulating electrode goes to the detecting electrode through the medium and if any material comes in between the two electrodes, then the electric field strength either increases or decreases. When that incoming material has a higher conductivity and permittivity than the previously present material, then the electric field strength increases, and as a result, the detected signal increases, otherwise it decreases [4].

Microfluidics is widely used for drug screening and library screening, owing to their capability to encapsulate single cells [5]. The separation of cells and the detection of their positions are essential for the wide application of microfluidics [6]. It offers the most important steps for a wide range of applications in biology and cell biology, especially in the case of heterogeneous mixtures [6]. Different methods can be used for droplet-based cell characterization like fluorescence detection which can detect microparticles, bacteria, yeast, and insect [7]. For the separations, the researchers use dielectrophoretic force widely which creates the same polarity in particles/droplets and separates from each other based on the created force [8]. The advantageous point in the case of impedance-based characterization and separation is that it needs less time and cost; also, real-time data is achieved. The application of impedance spectroscopy spans several fields from materials science to fuel cell research, corrosion phenomena, electrochemistry to biology, or heterogeneous cells position detection [9]–[13].

Cells characterization in microdroplet-based impedance spectroscopy has rarely been developed. Kemna et al. characterized viable and nonviable cells in the droplet, however, the droplet medium was significantly adjusted and reduced their medium conductivity as well as droplet size for better detection and characterizations, which could be not possible and appropriate in the range of other different cells in droplet growth [14]. On the other hand, cells in droplets using an impedance spectroscopy-based system were successfully detected and characterized using an unchanged droplet medium as presented in the previous works [15-16]. However, the problem is low sensitivity issues that the researchers face [17-18]. Sometimes, researchers convert the impedance to other mathematical terms like opacity to calculate it properly [18]. Sobahi et al. [17] had proposed highly sensitive impedance spectroscopy for differentiating four different cell concentrations in the droplets. Sobahi et al. further detected and characterized different inhomogeneous single cells in droplets using squeezed droplets [19].

In this work, an impedance spectroscopy-based microfluidic system for cells in the droplet had been modeled and simulated to characterize, identify, and count the cell encapsulated in the microdroplets using a normal medium and different sizes of the droplets.

2 Materials and Methods

Every cell has a different dielectric property and when a cell passes through the medium, it offers a unique value for electrical impedance to the electrodes based on its dielectric properties and frequency [20-21]. The equivalent circuit of a cell can be found in [20]. The impedance between two electrodes differs based on whether the droplet is empty or has a cell suspended in it. Further, the impedance between two electrodes can also differentiate between two cells having different

characteristic features. This impedance-based spectroscopic technique was used in this research to differentiate between two types of cells, i.e., wild-type yeast cells and mutant yeast cells.

For simulations, COMSOL Multiphysics 5.6, a Finite Element Method (FEM) based software was used. The detection region of the proposed design along with the cell model used are illustrated in Figure 1(a). The wild-type and mutant yeast cells model have been presented in Figures 1 (c) and 1 (d) along with the polystyrene bead in the droplet in Figure 1 (b). To determine the model's performance, microbeads were used. The only difference between the mutant and wild-type yeast cells is that the mutant yeast cell does not have any vacuole in the cytoplasm [18]. The electrodes used in the proposed model were designed as gold (Au) [21] with a width of 10µm and a height of 200nm. Also, 20nm of titanium was considered as an adhesion layer between the substrate and the gold electrode. As it had been characterized in the previous work [19], a 3.0V peak-to-peak alternating current was used at the stimulating electrode whereas the detecting electrode was grounded in this simulation.

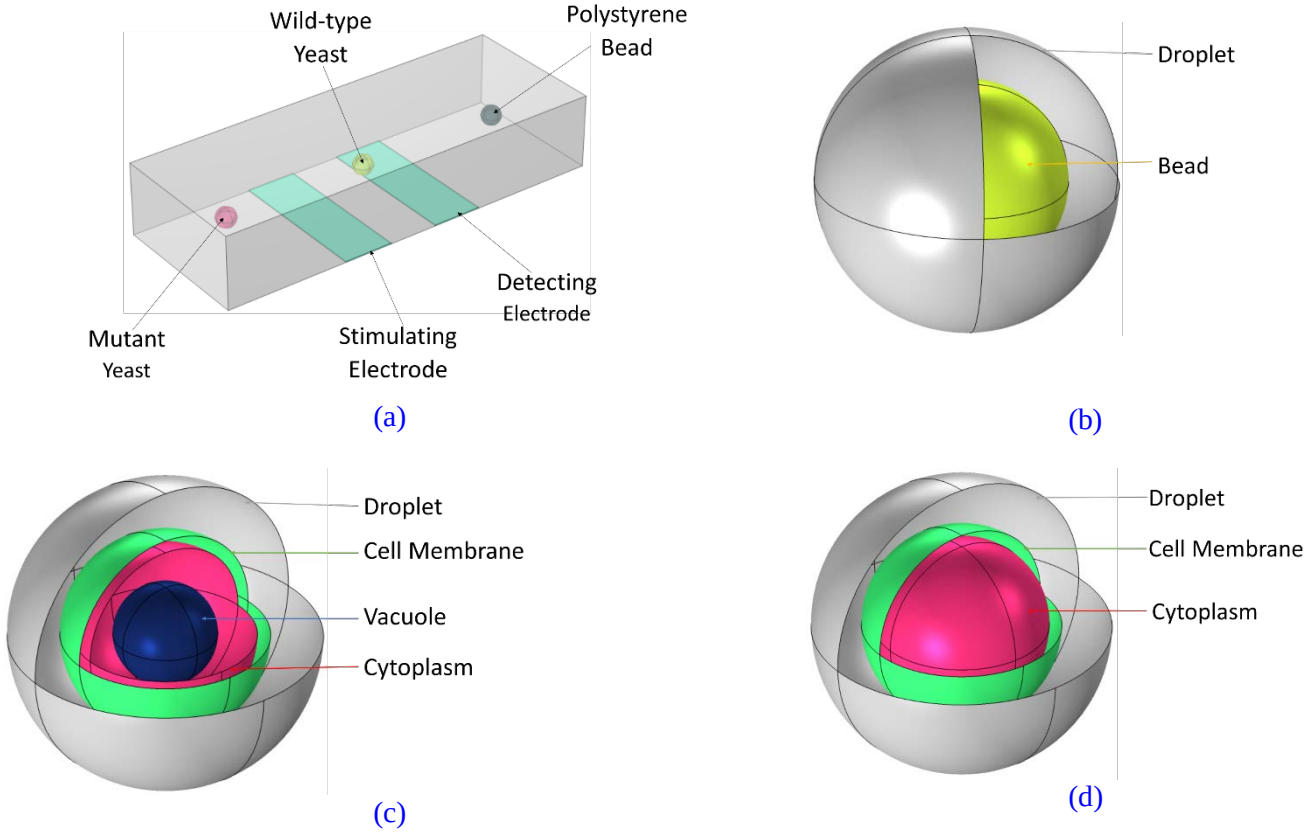

Figure 1: Illustration of the detection region of the microfluidic chip integrated with a pair of electrodes. (a) A 3D model of the sensing region along with the three particles (Wild-type yeast cell, Mutant yeast cell, and Polystyrene microbead) in the microchannel. (b) 3D view of the bead in the droplet. (c) 3D view of the wild-type yeast cell in the droplet. (d) 3D view of the mutant yeast cell in the droplet. The diameter for all these three particles was 4µm with the cell wall thickness of 250nm and the spherical vacuole's diameter of 2µm.

The droplet's medium conductivity, σ was modeled as 1.34 Sm^{-1} and the relative permittivity, ε_r was 80 as these are the typical values usually used for different applications [18] whereas the mineral oil used for the carrier had $\sigma = 0.175 Sm^{-1}$ with $\varepsilon_r = 2.1$. The cell membrane and the cytoplasm had the electrical properties as $\sigma = 0\,Sm^{-1}$, $\varepsilon_r = 5$ and $\sigma = 0.5\,Sm^{-1}$, $\varepsilon_r = 50$, respectively, whereas the vacuole's electrical properties were $\sigma = 1\,Sm^{-1}$, $\varepsilon_r = 50$ [11], [14]. The

diameter of the droplet was considered as 14µm, whereas the cell and bead diameter was only 4µm. The microbead's conductivity was 0.0012 Sm^{-1} with relative permittivity of 2.6 (Life Technologies Ltd, UK).

The impedances for the bead, wild-type yeast cell, and the mutant cell were analyzed for a band of frequencies from 1MHz to 500 MHz with an interval of 1KHz to determine the optimal frequency. The difference between the two conditions i.e., a droplet with a mutant and wild-type yeast cell was analyzed to find the optimum frequency. All four parts of impedance (amplitude, real, imaginary, and phase) were considered. However, it was observed that the amplitude impedance provided the best results to differentiate the cells in the droplets.

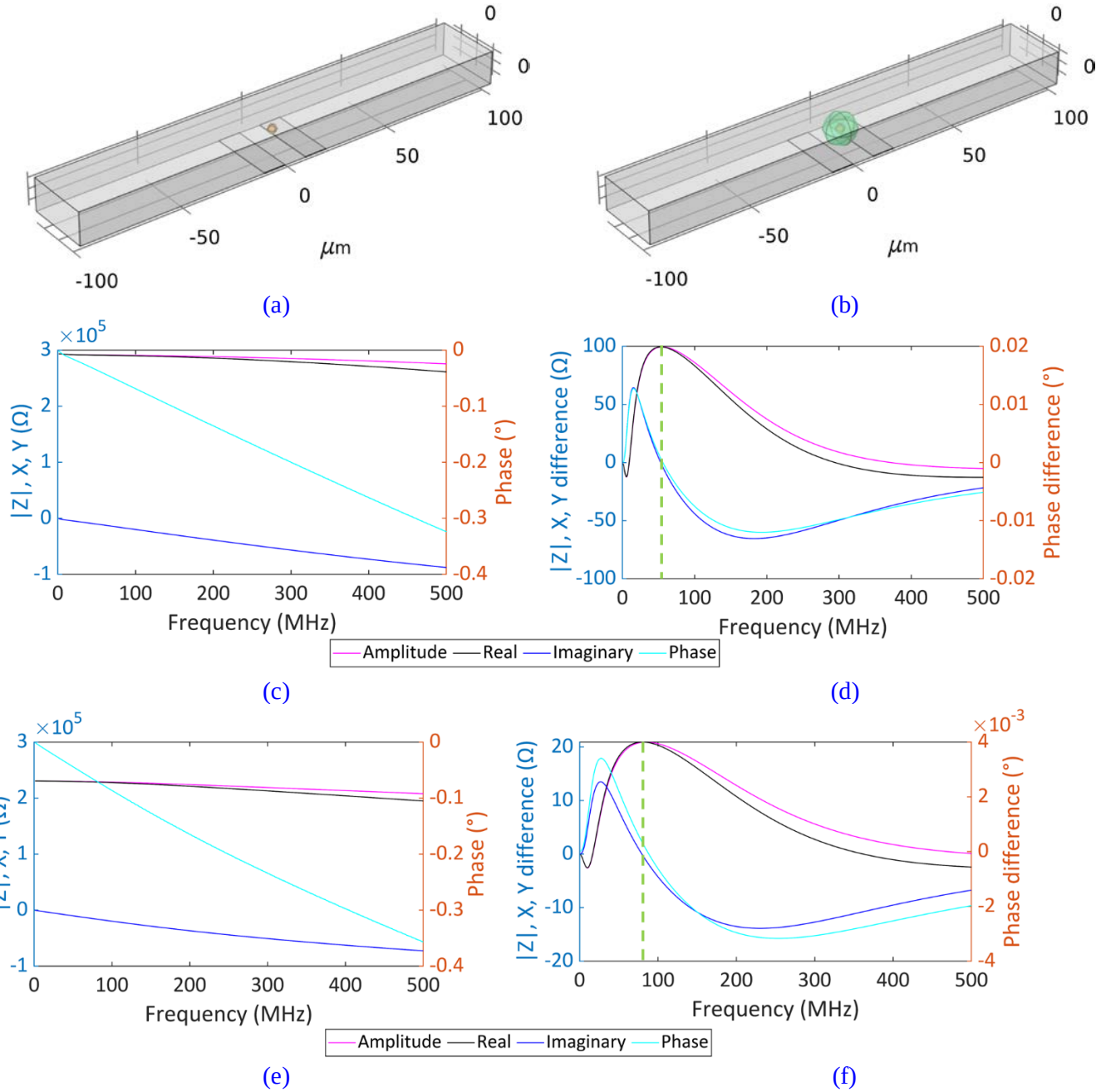

Figure 2: Optimum frequency selection: (a) Microfluidic channel with cell only (without droplet). (b) Microfluidic channel with cell in the droplet. (c) Wild-type yeast cell impedance at different frequencies without droplets. (d) Impedance difference for wild-type and mutant yeast cells at different frequencies without droplets. (e) Impedance offered by the wild-type yeast cell encapsulating in the droplets (f) Impedance difference for wild-type and mutant yeast cells encapsulated in droplets at different frequencies.

In Figures 2(a) and (b), the microfluidic channel along with the cell are presented without and with droplets respectively. The spherical-shaped droplet had been considered to find the optimum frequency where the cell (with and without droplet) was taken in between the electrodes. Figure 2 (c) presents the impedance (amplitude, real, imaginary, and phase) variations of wild-type yeast cells considering only the cell in the channel (without droplet). It was seen that for the wild-type yeast cell, the impedance decreased with the increment of frequency (Figure 2 (c)) following the common formula $X_c = 1/(2x\pi fC)$; where, X_c is the capacitive impedance, f is the applied frequency, and C is the capacitance [22]. The maximum impedance difference between the wild-type and mutant yeast cells was found at 55MHz frequency at no droplet condition (Figure 2 (d)) which means, 55MHz is the optimal frequency at no droplet condition.

The mineral oil used for the carrier in the simulation got touched the electrodes and offered huge impedance to the probes (used for impedance measurements). Since the cells need a suitable environment to live in, phosphate-buffered saline (PBS) had been used for that and once the PBS with the cell came in contact with the electrodes in the form of a droplet, the impedance decreased. Because of the droplet properties, the dielectric constant changed which caused less impedance and the optimum frequency shifted. The impact of the droplet material on the impedance and optimum frequency is seen in Figures 2(e) and 2(f). From Figure 2(e), it is seen that both the impedance real part and amplitude differences reached their maximum positions when 85MHz frequency was applied ($3V_{p\text{-}p}$ voltage). The maximum impedance difference of 99.42Ω was achieved at 55MHz frequency without droplet condition, which decreased to 20.91Ω once the droplet was considered. The frequency found as the optimum conditions both for with and without droplets are validated by the practical results found in [18] which stated that more than 50MHz frequency is required to get the accurate impedance from a small geometric shape like a vacuole.

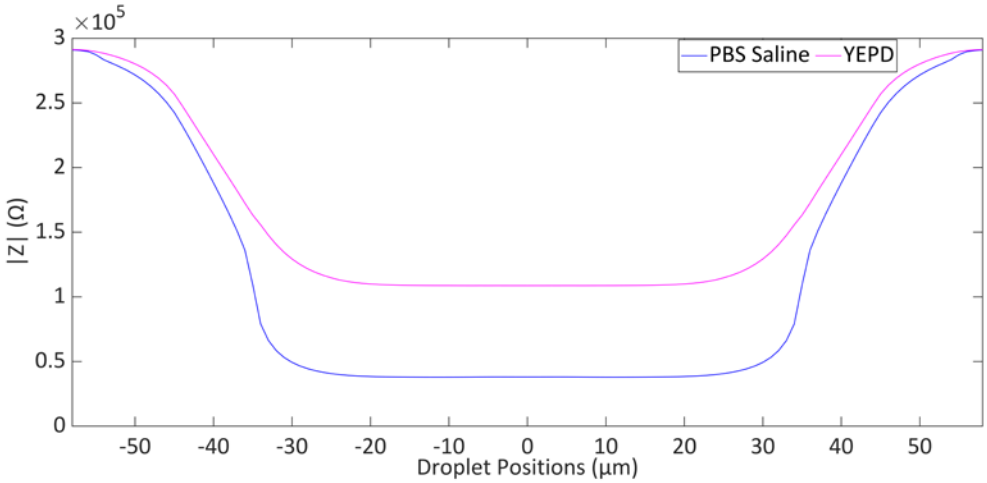

Figure 3: Diluting material's effect on base impedance selection: One complete cycle of impedance response once the droplet passed through the channel. For PBS, the base impedance was 38KΩ, which became 108.7KΩ for YEPD.

The liquid used for the dilution/surrounding material plays an important role in the baseline impedance. Figure 3 shows the impedance response for two different liquids i.e., PBS (used for this simulation) and yeast extract peptone dextrose (YEPD) encapsulating a single wild-type yeast cell

at the optimum frequency. For the YEPD, the electrical properties are $\sigma = 0.3\ Sm^{-1}$ and $\varepsilon_r = 80$ [23] which were $\sigma = 1.34\ Sm^{-1}$ and $\varepsilon_r = 80$ for PBS [18]. It is seen that the higher the conductivity, the lower will be the baseline impedance (with constant relative permittivity).

After obtaining the optimum frequency (85MHz), the microdroplets had been flown through the channel of 200µm in length with 1µm in every step. The microfluidic channel depth and height were 30µm and 15µm respectively. All simulations had been conducted in a complete electrical and magnetic insulation environment. MATLAB software had been used for data analysis and graphical representation.

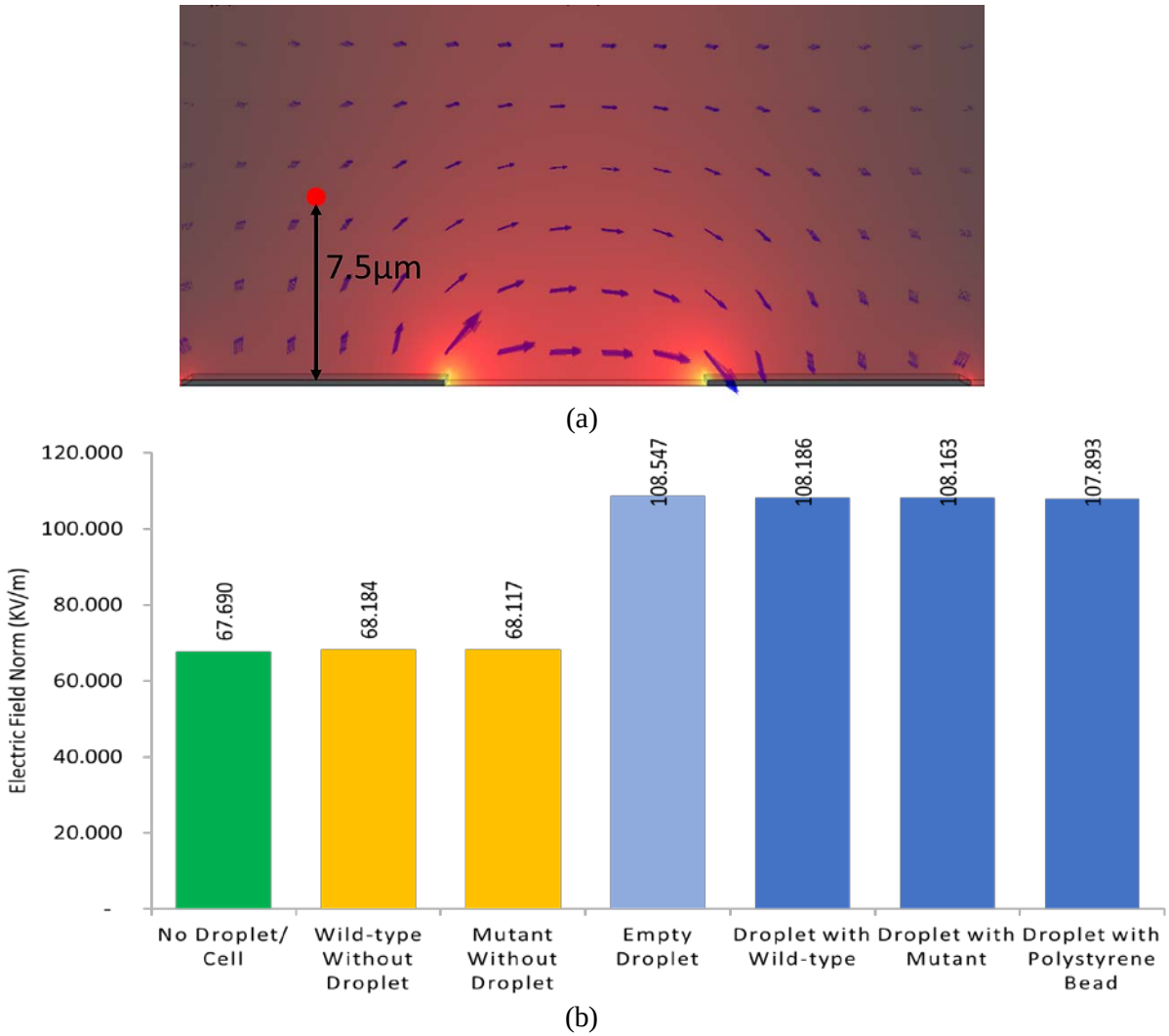

Figure 4: Electric field change for the droplets: (a) Side-view of the 3D detection region. The electric field came out from the stimulating electrode and entered the detecting electrode. (b) Electric field changes for cells/beads with and without droplets were present in the detection region. The electric field had been calculated at 7.5µm above the stimulating electrode.

The electric field (E. field) norm had been changed for the presence of the droplets with different conditions presented in Figure 4. In Figure 4 (a), the E. field norm is shown that goes from the stimulating electrode to the detecting electrode. The E. filed norms were taken at 85MHz frequency and $3V_{p\text{-}p}$ AC voltage. When there was no droplet/cell in the detection region, the oil touched the electrodes, and at that time, the E. field norm was less ($67.690 KVm^{-1}$) which increased slightly when the cells were present in between the electrodes (Figure 3 (b)). The E. field norm

reached 68.184KVm^{-1} and 68.117KVm^{-1} for the wild-type and mutant yeast respectively. Once the empty droplet came in between the electrodes, the E. field norm increased to 108.547KVm^{-1}. It again decreased slightly when the droplet contained any yeast cells or polystyrene bead and reached its minimum (107.893KVm^{-1}) when it encapsulated the bead shown in Figure 4 (b).

3 Results and Discussion

It is seen from Figure 5 that at three different conditions of droplets (i.e., a droplet with polystyrene bead, mutant yeast, and wild-type yeast), the impedances were different. The carrier itself offered a fixed impedance when there was no cell/droplet present in between the electrodes which decreased once the droplets passed and reached their minimum when it was in the middle of two electrodes (Figure 5(b)). Figure 5(c) shows the detected signal of amplitude impedance in an enlarged view when the droplets contained a single cell. It is seen that though the impedance reached its minimum amplitude at the middle positions, the droplet with bead offered more impedance compared to the yeast cells. As wild-type yeast cells are more conductive compared to the other two particles, they offered minimal impedance. The droplets containing cells in the microfluidic channel flew as shown in Figure 2(b).

From the impedance signal offered by the particles, it is possible to differentiate different types of cells. In Figure 5, the impedance difference between the bead and mutant yeast is 216.2Ω and for the mutant and wild-type yeast, a 20.91Ω difference was found.

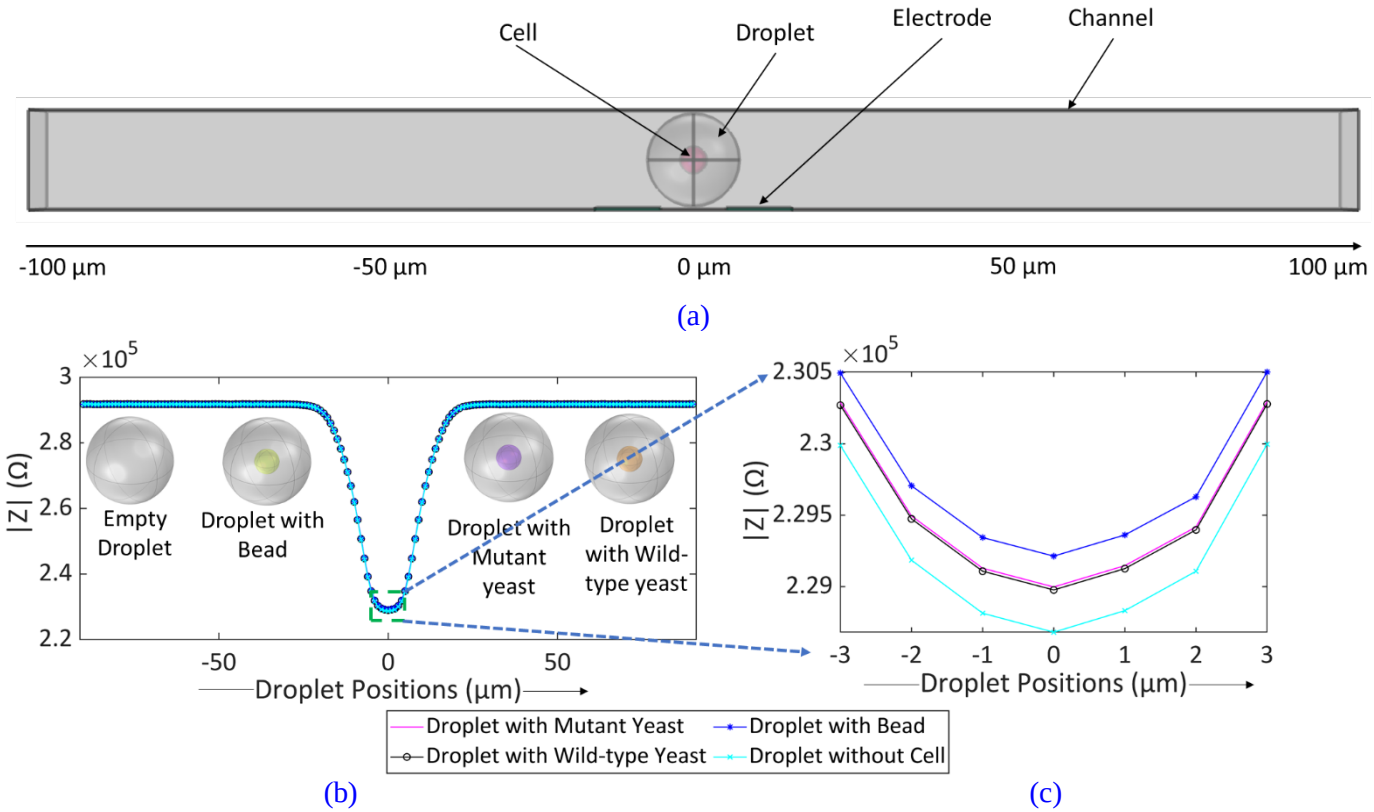

Figure 5: (a) Sideview of the microfluidic channel (b) Impedance of four conditions of droplet i.e., empty droplet, a droplet with mutant yeast, a droplet with wild-type yeast, and droplet with bead. (c) Enlarged view of the minimum impedances.

For increasing the number of cells in the droplet, the impedance increases as the cell are less conductive than the droplets. The cell orientation in the droplet is shown in Figure 6 along with the

impedance responses. For the spherical-shaped droplet, the single mutant cell offered 47.14Ω which increased with the number of cells increase in the droplet. So, the proposed model successfully counted the number of cells in the droplet. In Figures 6(a) and 6(c), the full cycle impedance responses are shown for wild-type and mutant yeast cells respectively whereas Figures 6(b) and 6(d) show the respective enlarged views of the impedance for cell detection, counting, and differentiation.

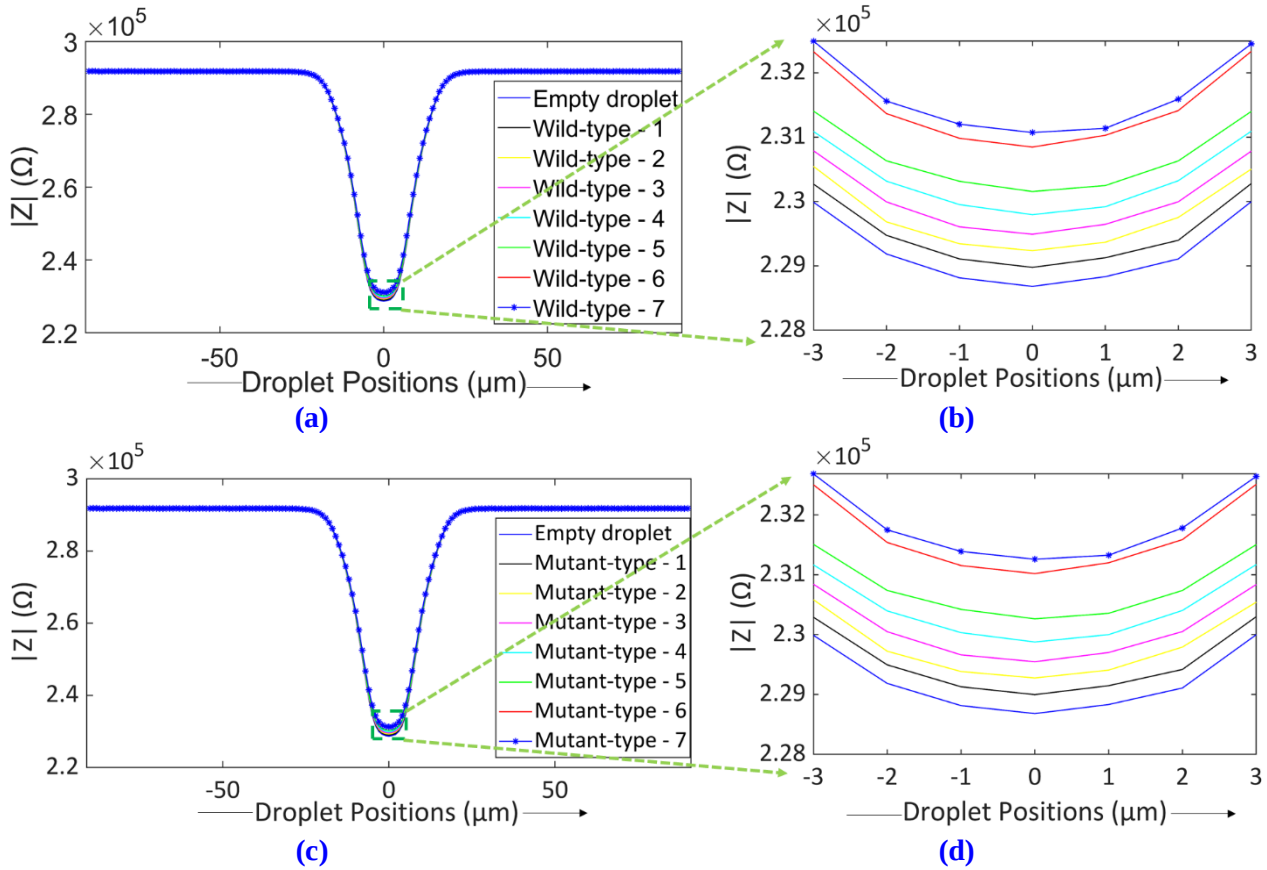

Figure 6: Impedance offered for the different number of cells in the droplets; 0 is the middle point between two electrodes. (a) The impedance of 1-7 numbers of wild-type yeast cells in the droplet along with cell orientations in the droplets. (b) Enlarged view of the impedances for the different numbers of wild-type yeast encapsulated in droplets. (c) The impedance of 1-7 numbers of mutant yeast cells in the droplet along with cell orientations. (d) Enlarged view of impedances of the different number of mutant cells in the droplets.

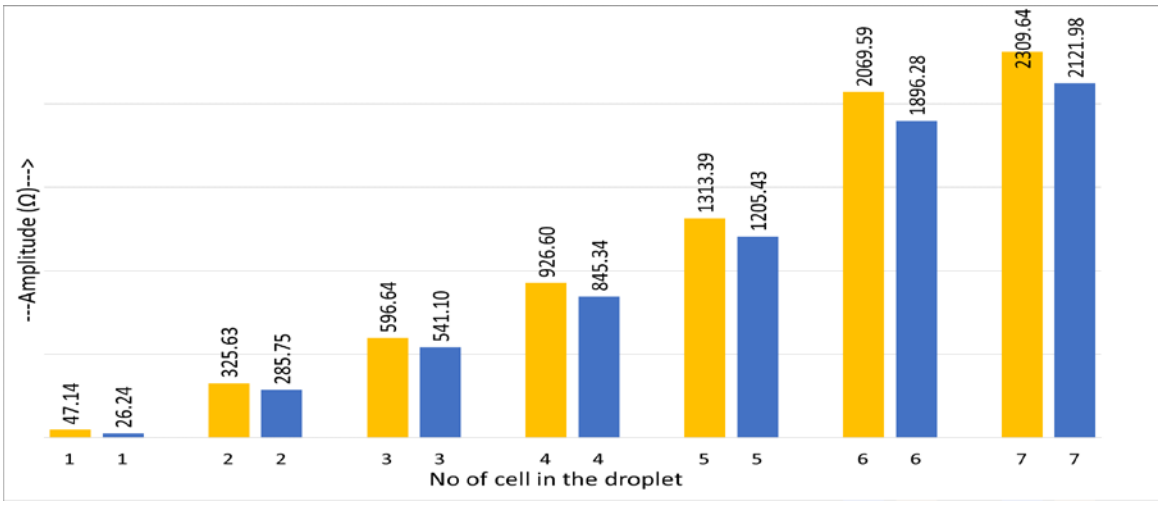

Figure 7: Peak impedance differences between different numbers of wild-type and mutant yeast cells in the spherical droplets with the baseline impedance of 228.95KΩ. The peak impedances increased due to the increase of cell numbers in the droplets.

Similarly, this model can differentiate between wild-type yeast, and mutant yeast, illustrated in Figure 7 where it is seen that the maximum impedances offered by the different number of mutant and wild-type cells encapsulated in the droplets are different.

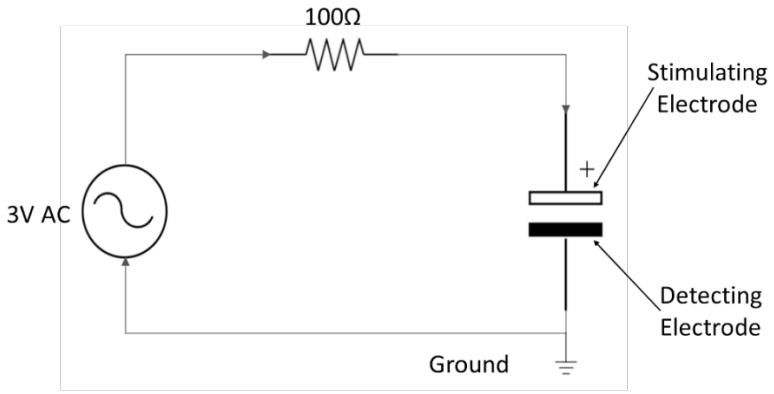

Figure 8: The Equivalent circuit diagram for cell impedance analysis encapsulated in the droplets.

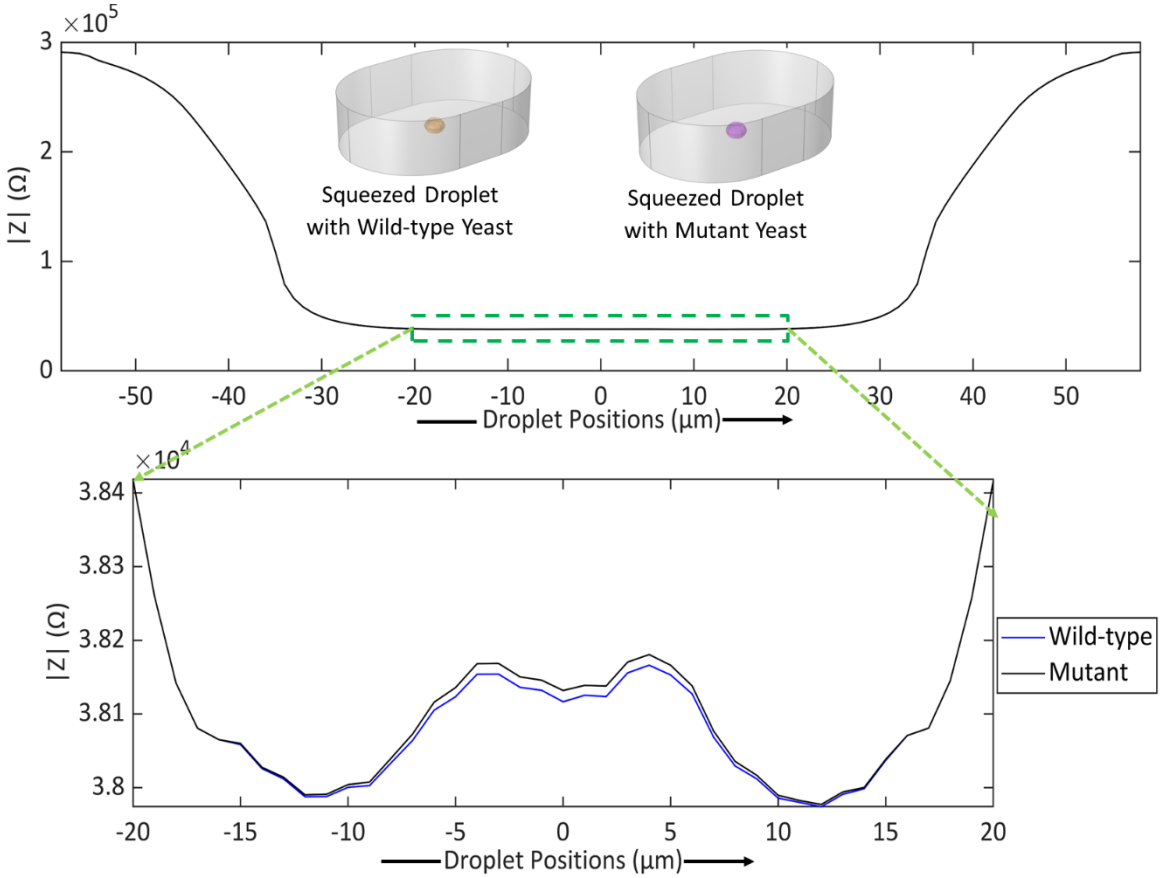

Figure 9: Impedance responses for Wild-type and Mutant yeast cells in the squeezed droplets along with the cell orientation. An enlarged view of the cell impedance for detection. Both cells have similar impedance responses, however, the mutant yeast cell's impedance amplitude is 14.42Ω more than the wild-type yeast cell.

As the vacuole is present in the wild-type yeast, its impedance is more than the mutant cell. As in the practical case, the droplet is not always of the spherical shape and a squeezed shape (as the channel) can be formed [24-25] which also increases the sensitivity [25] of the detection. The T-junction is generally used for microfluidic droplet creation that breaks up the droplet into the squeezed shape using the shear force and squeezing mechanism [7], [26]. This aspect was, therefore, considered, simulated, and compared. In Figure 8, the equivalent circuit diagram of the

system is shown. A 100Ω resistance was considered in series with the stimulating electrode and as mentioned earlier, the other electrode was used as a detecting electrode. The squeezed droplets' dimensions were taken as (Length x Depth x Height) = 80µm x 29µm x 15µm. As the channel height was the same as the size of the droplets, it forced the droplets to be squeezed. In that case, the peak was different from the spherical droplet encapsulated cells as the squeezed droplets have greater volume (34800.0 μm^3 for squeezed and 1436.3 μm^3 for spherical droplets). Both the wild-type and mutant yeast cells' impedances increased when the cells were between the electrodes shown in Figure 9.

In Figure 9, a complete impedance cycle is presented with the mutant and wild-type yeast orientations in the squeezed droplets along with an enlarged view for analysis and detection. It is seen that following the E. field norm in figure 4 (a), the impedance in Figure 9 changed which was not noticed for the spherical droplets like Figures 5 and 6 as the spherical droplet's area and volume were less.

Figure 10 shows the impedance responses in squeezed droplets for various numbers of wild-type and mutant yeast cells at a time. The full cycle impedance of wild-type yeast encapsulated in squeezed droplets is shown in Figure 10 (a). The enlarged view for signal detection is also presented where the amplitude impedances with a narrow range of x-axis (-15 to 15) are illustrated to show the impedance variation as the number of droplets changes. Figure 10 (b) depicts the entire cycle impedance as well as an enlarged view of mutant-type yeast. Maximum seven numbers cells fitted into the droplet serially. The impedance increased once the number of cells in the droplet increased due to the change in the corresponding electric field. In Figure 10, the cell numbers in the droplets had been increased one by one in a series that worked as a series resistor for current to pass from one stimulating electrode to the detecting electrode.

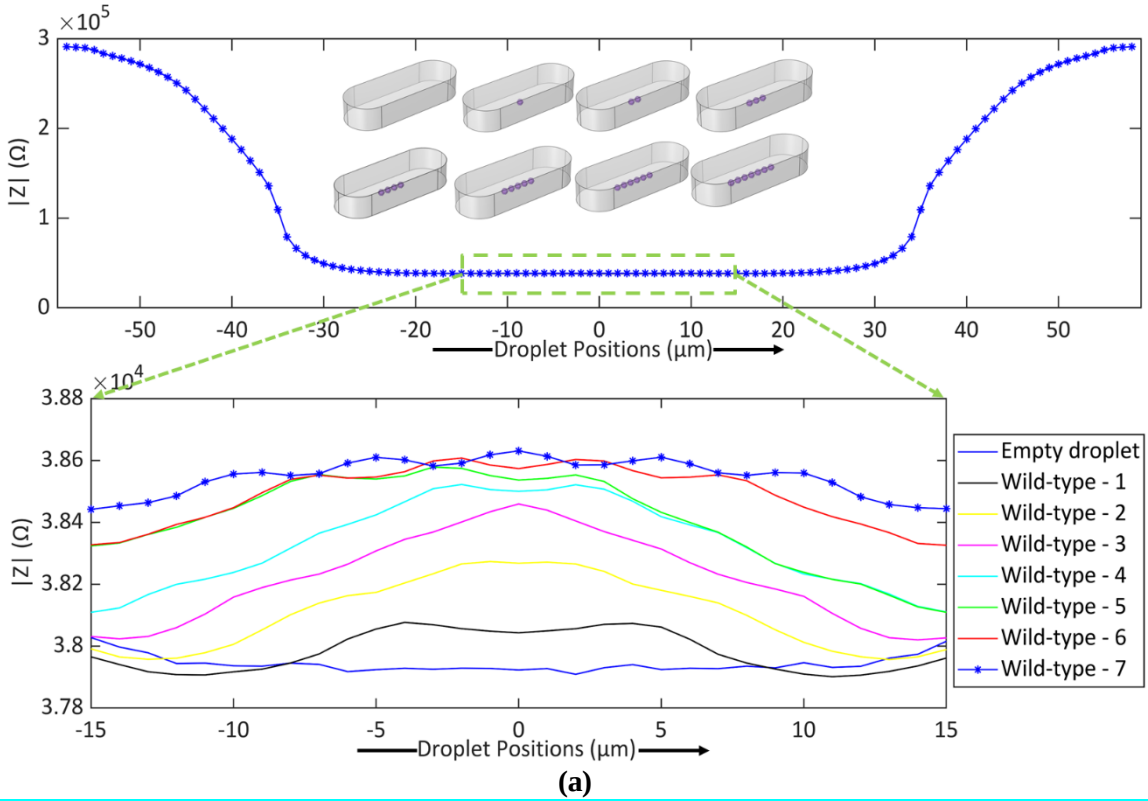

(a)

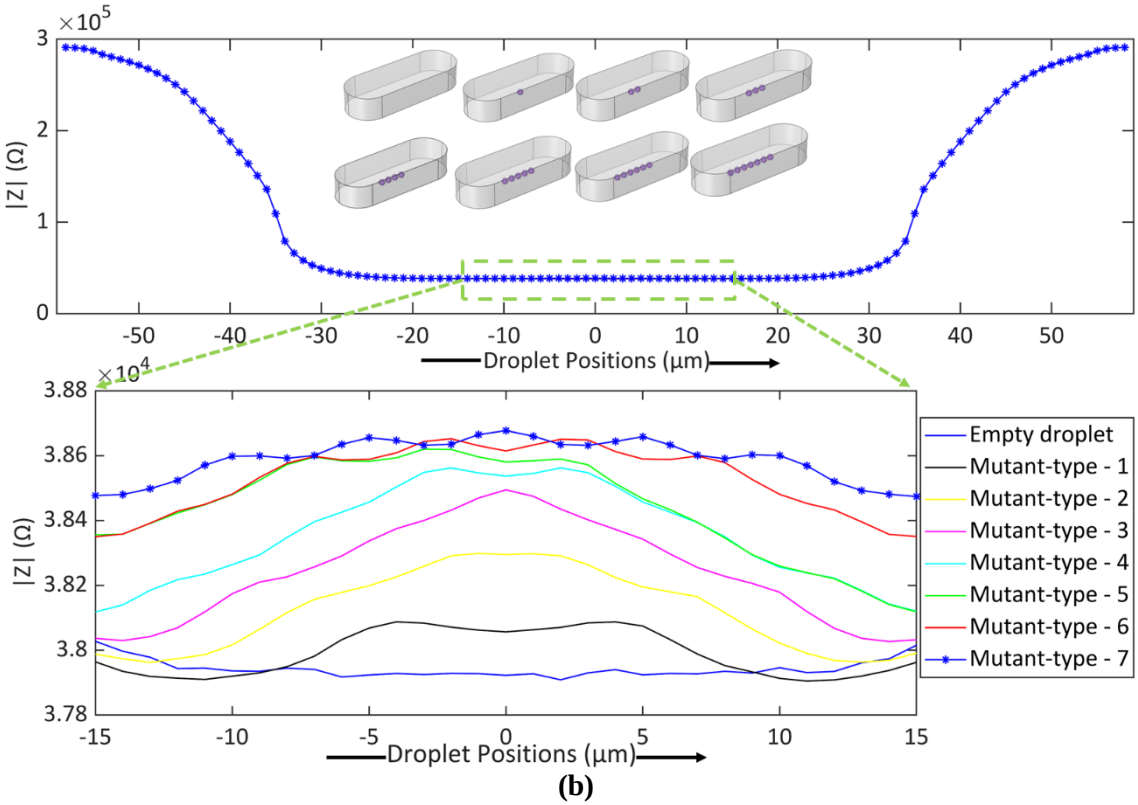

(b)

Figure 10: Impedance offered for the different number of cells in the squeezed-shaped droplets; 0 is the middle point of two electrodes. (a) The impedance of 1-7 numbers of wild-type yeast cells in the droplet along with cell orientations. Enlarged view of the impedances for the different number of mutant encapsulated droplets. (b) The impedance of 1-7 numbers of wild-type yeast cells in the droplet along with cell orientations. Enlarged view of impedances of the different number of wild-type cells in the droplets.

The maximum impedances for different numbers of mutant and wild-type yeast encapsulated in the squeezed droplets are presented in Figure 11. As the volume of the droplets increased for the squeezed shape, the baseline impedance had also been changed and it decreased to 38KΩ, which was the peak impedance for empty droplets.

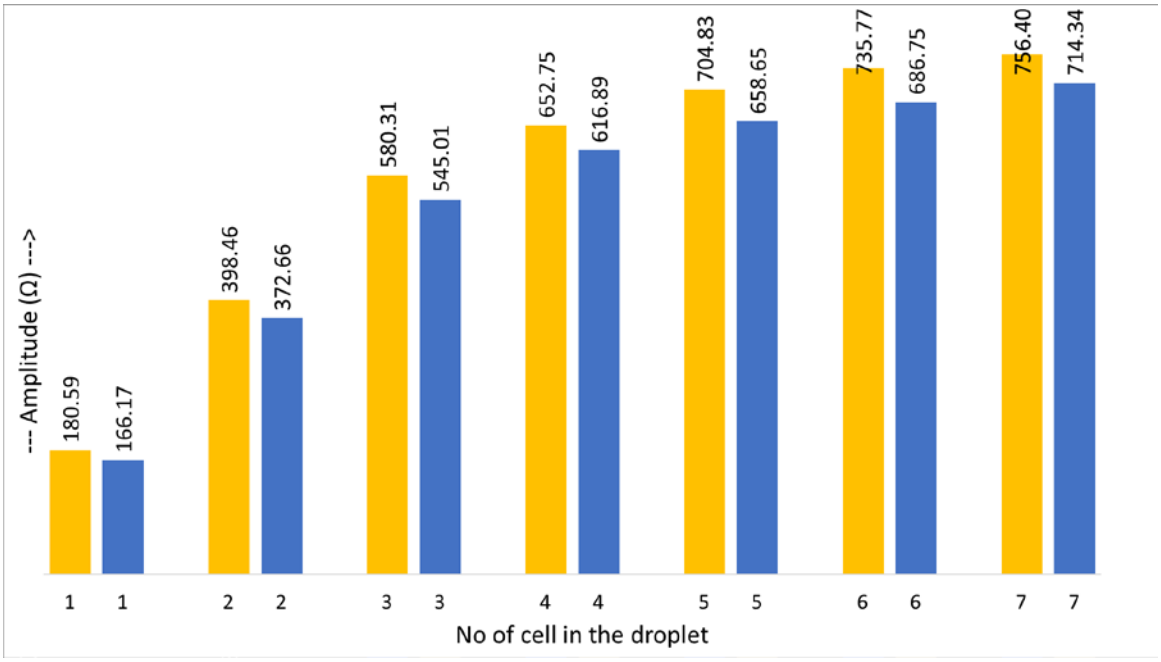

Figure 11: Peak impedances for different numbers of mutant and wild-type yeast cells in the squeezed droplets. Impedance increases due to the increase of cell number maintaining differences between wild-type and mutant.

This perspective is to show the cells having gaps between them. The previous case was NOT a cycle, but the case of having the cells without gaps since the cycle in yeast cells generates a daughter and the mother until they are disconnected from each other. Figure 12 shows the impedance response for two wild-type and mutant yeast cells present in the same droplet. In this case, a 30µm distance was kept between two cells for good visualization of the signal as the electrodes' electric field was spread up to 30µm (electrode width was 10µm each and the gap between them was 10µm). The enlarged view of the signal detection and separation is also shown along with the full-cycle impedance responses. For the peak in Figure 12, the impedance difference between two cells is ≈ 15Ω which is easily differentiable. As shown in the previous sections, in this case also the impedance responses for two yeast cells were similar but for both peaks, mutant yeast offered more impedance than the wild-type.

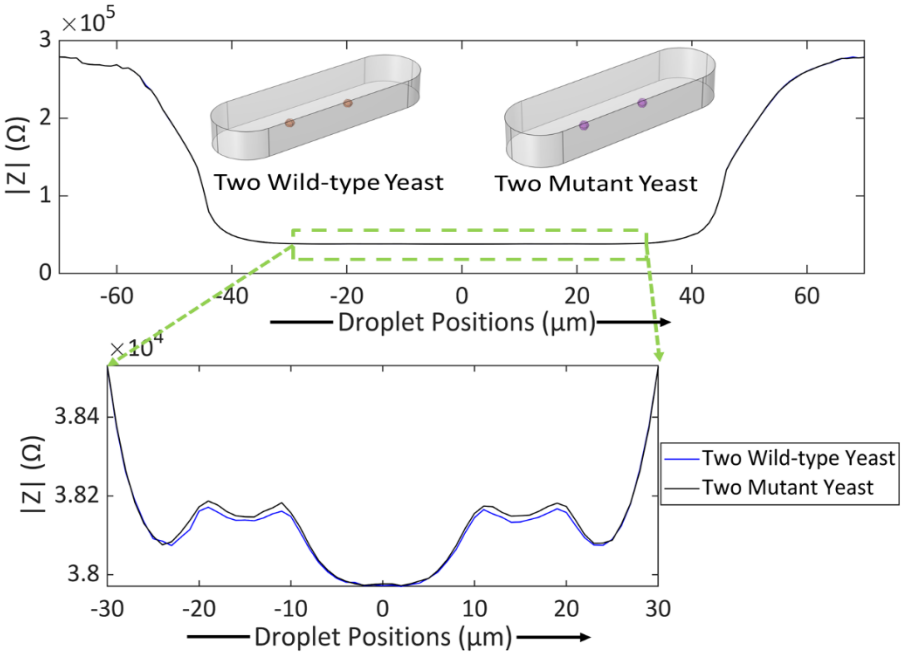

Figure 12: Impedance response for two cells present in the same droplet. The impedance peak for mutant cells is higher than the peak found for wild-type yeast cells.

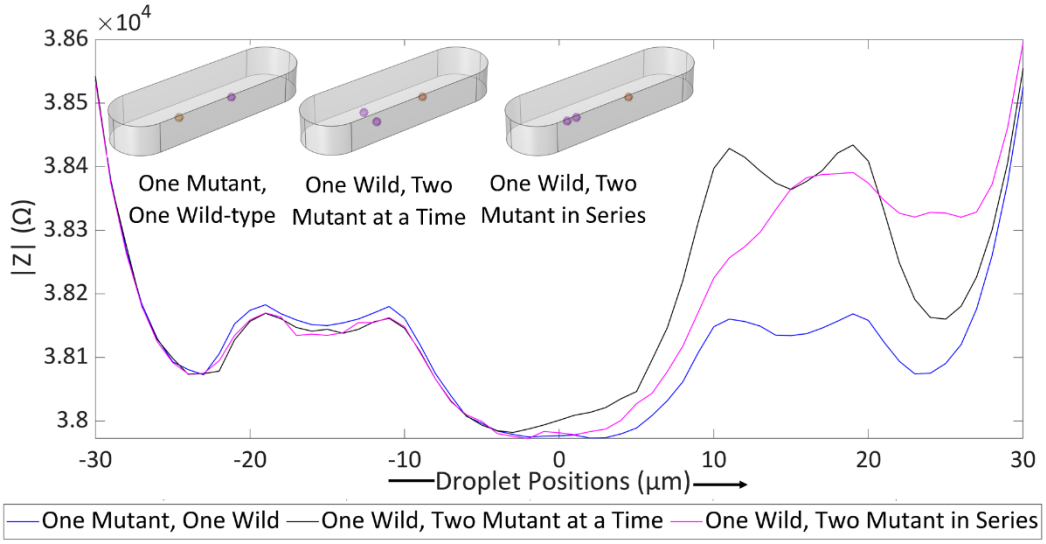

Figure 13: Impedance response for different types of cells present in the same droplet.

In another case, it is also possible that two different types of yeast cells are present in the same droplet and multiple cells can be present in the droplet at a time or one after another. Figure 13 shows the impedance responses considering the above three conditions. The impedance signal for one mutant and one wild type showed a difference of ≈ 15Ω which rose to 246Ω once two mutant cells presented at the same time. But the signal changed if those mutant yeasts were present in the detection region serially (pink color). In that case, the signal is like Figure 10 (b) for the mutant cell but no change for the wild-type cell.

Impedance responses for multiple cells present in the droplets shown in Figures 12 and 13 (with no baseline) indicate that cells can be easily identified and characterized based on their impedance signals. It was also observed that differentiating two types of cells based on impedance became easier for squeezed droplets. Figure 14 depicts the maximum impedance difference for a single cell in both types of droplets.

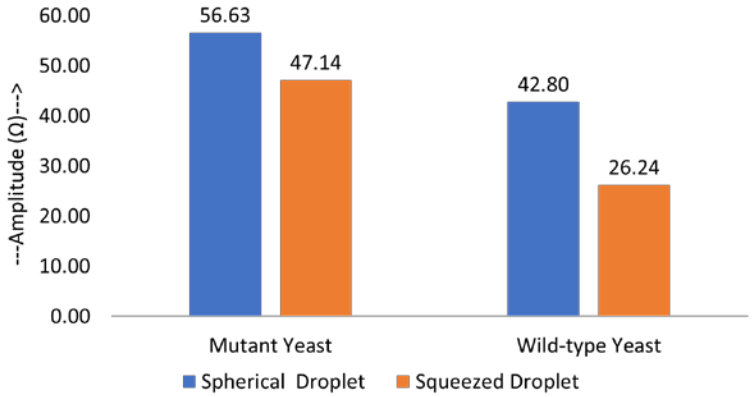

Figure 14: The peak impedance offered by the spherical and squeezed droplets with one mutant and wild-type yeast cell.

The impedance difference decreased between mutant and wild-type yeast encapsulated droplets for squeezed shape and reached 14.42Ω which was 20.91Ω for the spherical droplets. The baseline impedance was observed to be different for different shaped droplets as the droplet itself offered a specific impedance; but in all the conditions, the mutant and wild-type yeast were identified and counted based on the impedance offered.

4 Conclusion

Label-free, non-contact microfluidic impedance spectroscopy-based systems for cells in droplet detection and characterization were modeled and simulated. The simulation results showed successful differentiation between the mutant and wild-type yeast cells encapsulated in that droplet. The optimum frequency for the cell identification and differentiation was chosen by analyzing a frequency band up to 500MHz and it was found that at the optimum frequency, the polystyrene bead, wild-type yeast, mutant yeast, and empty droplet provided different impedances. Two different droplet sizes and schemes were developed and compared namely, spherical and squeezed droplets. The model demonstrated two different types of responses for series and separately placed cells in the droplets. The model also showed that different materials of particles encapsulated in droplets could be detected and discriminated based on their dielectric properties.

Likewise, the model can be used to discriminate among the different numbers of cells encapsulated in droplets. Therefore, this microsystem model can be utilized for a range of different applications related to cell identification, separation, and characterizations.

5 Availability of Data and Material

Data can be made available by contacting the corresponding author.

6 Acknowledgement

This research work was funded by institutional Fund Projects under grant no.(IFPRC-049-135-2020). Therefore, the authors gratefully acknowledge technical and financial support from the Ministry of Education and King Abdulaziz University, Jeddah, Saudi Arabia.

7 References

[1] Čičmanec, P. (1971). Cavity perturbation method for measurement of permittivity and conductivity of medium lossy semiconductors and dielectrics. *Solid-State Electronics, 14*(2), 153-166.

[2] Barthel, J., Bachhuber, K., Buchner, R., & Hetzenauer, H. (1990). Dielectric spectra of some common solvents in the microwave region. Water and lower alcohols. *Chemical physics letters, 165*(4), 369-373.

[3] Rouleau, J. F., Goyette, J., Bose, T. K., & Frechette, M. F. (2000). Performance of a microwave sensor for the precise measurement of water vapor in gases. *IEEE Transactions on Dielectrics and Electrical Insulation, 7*(6), 825-831.

[4] Tai, C. C. (2000). Characterization of coatings on magnetic metal using the swept-frequency eddy current method. *Review of Scientific Instruments, 71*(8), 3161-3167.

[5] Teh, S. Y., Lin, R., Hung, L. H., & Lee, A. P. (2008). Droplet microfluidics. *Lab on a Chip, 8*(2), 198-220.

[6] Wang, H., Sobahi, N., & Han, A. (2017). Impedance spectroscopy-based cell/particle position detection in microfluidic systems. *Lab on a Chip, 17*(7), 1264-1269.

[7] Lichtman, J. W., & Conchello, J. A. (2005). Fluorescence microscopy. *Nature methods, 2*(12), 910-919.

[8] Ahn, K., Kerbage, C., Hunt, T. P., Westervelt, R. M., Link, D. R., & Weitz, D. A. (2006). Dielectrophoretic manipulation of drops for high-speed microfluidic sorting devices. *Applied Physics Letters, 88*(2), 024104.

[9] Wang, H., Sobahi, N., & Han, A. (2017). Impedance spectroscopy-based cell/particle position detection in microfluidic systems. *Lab on a Chip, 17*(7), 1264-1269.

[10] Sheng, W., Gasteiger, H. A., & Shao-Horn, Y. (2010). Hydrogen oxidation and evolution reaction kinetics on platinum: acid vs alkaline electrolytes. *Journal of The Electrochemical Society, 157*(11), B1529.

[11] Haandbæk, N., Bürgel, S. C., Rudolf, F., Heer, F., & Hierlemann, A. (2013, June). Microfluidic impedance cytometer for characterization of subcellular morphology of single cells. In *2013 Transducers & Eurosensors XXVII: The 17th International Conference on Solid-State Sensors, Actuators and Microsystems (TRANSDUCERS & EUROSENSORS XXVII)* (pp. 1314-1317). IEEE.

[12] Nishikata, A., Ichihara, Y., & Tsuru, T. (1996). Electrochemical impedance spectroscopy of metals covered with a thin electrolyte layer. *Electrochimica Acta*, 41(7-8), 1057-1062.

[13] N. Nasir, N., & Al Ahmad, M. (2020). Cells electrical characterization: dielectric properties, mixture, and modeling theories. *Journal of Engineering*, 2020.

[14] Kemna, E. W., Segerink, L. I., Wolbers, F., Vermes, I., & van den Berg, A. (2013). Label-free, high-throughput, electrical detection of cells in droplets. *Analyst, 138*(16), 4585-4592.

[15] Sobahi, N. M. A. (2014). *Development of High-Throughput Microfluidic Impedance Spectroscopy Platform for Analyzing Microdroplets in Droplet Microfluidic System*. Doctoral dissertation.

[16] Butler, D., Goel, N., Goodnight, L., Tadigadapa, S., & Ebrahimi, A. (2019). Detection of bacterial metabolism in lag-phase using impedance spectroscopy of agar-integrated 3D microelectrodes. *Biosensors and Bioelectronics*, 129, 269-276.

[17] Sobahi, N., et al. (2014). A high-throughput impedance spectroscopy platform for characterizing the concentration of cells within microdroplets. *18th International Conference on Miniaturized Systems for Chemistry and Life Sciences, MicroTAS 2014*, pp. 1963–1965, 2014.

[18] Haandbæk, N., Bürgel, S. C., Heer, F., & Hierlemann, A. (2014). Characterization of subcellular morphology of single yeast cells using high-frequency microfluidic impedance cytometer. *Lab on a Chip*, 14(2), 369-377.

[19] Sobahi, N., et al. (2016). Discrimination of droplets containing single cultured filamentous fungal cell using impedance spectroscopy. *20th International Conference on Miniaturized Systems for Chemistry and Life Sciences, MicroTAS 2016*, pp. 1168–1169.

[20] Sun, T., & Morgan, H. (2010). Single-cell microfluidic impedance cytometry: a review. *Microfluidics and Nanofluidics*, *8*(4), 423-443.

[21] Foster, K. R., & Schwan, H. P. (1986). *Dielectric properties of tissues*. CRC handbook of biological effects of electromagnetic fields, 27-96.

[22] Boylestad, R. L., & Nashelsky, L. (2012). *Electronic devices and circuit theory*. Prentice Hall.

[23] Sobahi, N., & Han, A. (2020). High-throughput and label-free multi-outlet cell counting using a single pair of impedance electrodes. *Biosensors and Bioelectronics*, 166, 112458.

[24] Kemna, E. W., Segerink, L. I., Wolbers, F., Vermes, I., & van den Berg, A. (2013). Label-free, high-throughput, electrical detection of cells in droplets. *Analyst*, *138*(16), 4585-4592.

[25] Sobahi, N. M. A. (2017). *Development of high-throughput impedance spectroscopy-based microfluidic platform for detecting and analyzing cells and particles*. Doctoral dissertation.

[26] Sivasamy, J., Wong, T. N., Nguyen, N. T., & Kao, L. T. H. (2011). An investigation on the mechanism of droplet formation in a microfluidic T-junction. *Microfluidics and nanofluidics*, 11(1), 1-10.

Shabbir Chowdhury is a Master's Student at the Department of Electrical and Computer Engineering, King Abdulaziz University, Saudi Arabia. He got a Bachelor's degree in Electrical and Electronic Engineering from Bangabandhu Sheikh Mujibur Rahman Science and Technology University, Bangladesh. His research is associated with Microfluidics, Cell Separations, Micro-Droplet Technology.

Professor Dr. Mohammad Asif Hussain is a Professor at the Department of Electrical and Computer Engineering, King Abdulaziz University, Saudi Arabia. He got his Ph.D. degree from the Indian Institute of Technology Bombay, India. His postdoctoral research experiences include as STA fellow in Japan and USA. His research includes Functional Materials, Tissue Engineering, Nanoimaging and Nanomechanical Characterization of Nano/micro Features of Synthetic Materials. Dr. Hussain's research also spans Developing Sensing Platforms for Toxicology and Pharmacology pursuits including Microfluidics.

Dr. Nebras Sobahi is an Assistant Professor at King Abdulaziz University. Dr. Sobahi received his B.Sc. and M.Sc. degrees in Electrical Engineering from King Abdulaziz University, and a second M.Sc. and a Ph.D. in Electrical Engineering from Texas A&M University, USA. His research encompasses Nano and Microfabrication, Lithography, Deposition, High Sensitive Impedance Spectroscopy Measurement, and High-throughput Detection Microsystems. Also, his engineering professional focuses on Nano and Microfabrication Process, Microfluidics, MEMS and BIOMEMS, Signal Processing, and Semiconductors.